Significant production of $ClNO_2$ and possible source of Cl_2 from N_2O_5 uptake at a suburban site in eastern China

Men Xia[a], Xiang Peng[a], Weihao Wang[a], Chuan Yu[a], Peng Sun[b], Yuanyuan Li[b], Yuliang Liu[b], Zhengning Xu[b], Zhe Wang[a, c], Zheng Xu[b], Wei Nie[b], Aijun Ding[b], and Tao Wang[a,*]

[a] Department of Civil and Environmental Engineering, The Hong Kong Polytechnic University, Hong Kong, China

[b] Joint International Research Laboratory of Atmospheric and Earth System Sciences, School of Atmospheric Sciences, Nanjing University, Nanjing, 210023, China

[c] Now at Division of Environment and Sustainability, Hong Kong University of Science and Technology, Hong Kong, China

* *Correspondence to*: Tao Wang (cetwang@polyu.edu.hk)

Abstract

$ClNO_2$ and Cl_2 can affect atmospheric oxidation and thereby the formation of ozone and secondary aerosols, yet their sources and production mechanisms are not well understood or quantified. In this study we present field observations of $ClNO_2$ and Cl_2 at a suburban site in eastern China during April 2018. Persistent high levels of $ClNO_2$ (maximum ~3.7 ppbv; 1 min average) were frequently observed at night, due to the high $ClNO_2$ yield ($\varphi(ClNO_2)$, 0.56 ± 0.20) inferred from the measurements. The $\varphi(ClNO_2)$ value showed a positive correlation with the $[Cl^-]/[H_2O]$ ratio, and its parameterization was improved at low to median yields (0~0.75) by the incorporation of $[Cl^-]/[H_2O]$ and the suppression effect of aerosol organics. $ClNO_2$ and Cl_2 showed a significant correlation on most nights. We show that the Cl_2 at our site was more likely a co-product with $ClNO_2$ from N_2O_5 uptake on acidic aerosols that contain chloride, than being produced by $ClNO_2$ uptake as previously suggested. We propose a mechanism in which NO_2^+ can react with Cl^- to produce Cl_2 and $ClNO_2$ simultaneously. Under a new framework which regards Cl_2, $ClNO_2$, and nitrate as products of N_2O_5 uptake, the Cl_2 yield ($\varphi(Cl_2)$) was derived using ambient data. $\varphi(Cl_2)$ exhibited significant correlations with $[Cl^-]$ and $[H^+]$, based on which a parameterization of $\varphi(Cl_2)$ was developed. The derived parameterizations of $\varphi(ClNO_2)$ and

φ(Cl_2) can be used in models to evaluate the nighttime production of $ClNO_2$ and Cl_2 and their impact on the next day's photochemistry.

Graphical abstract

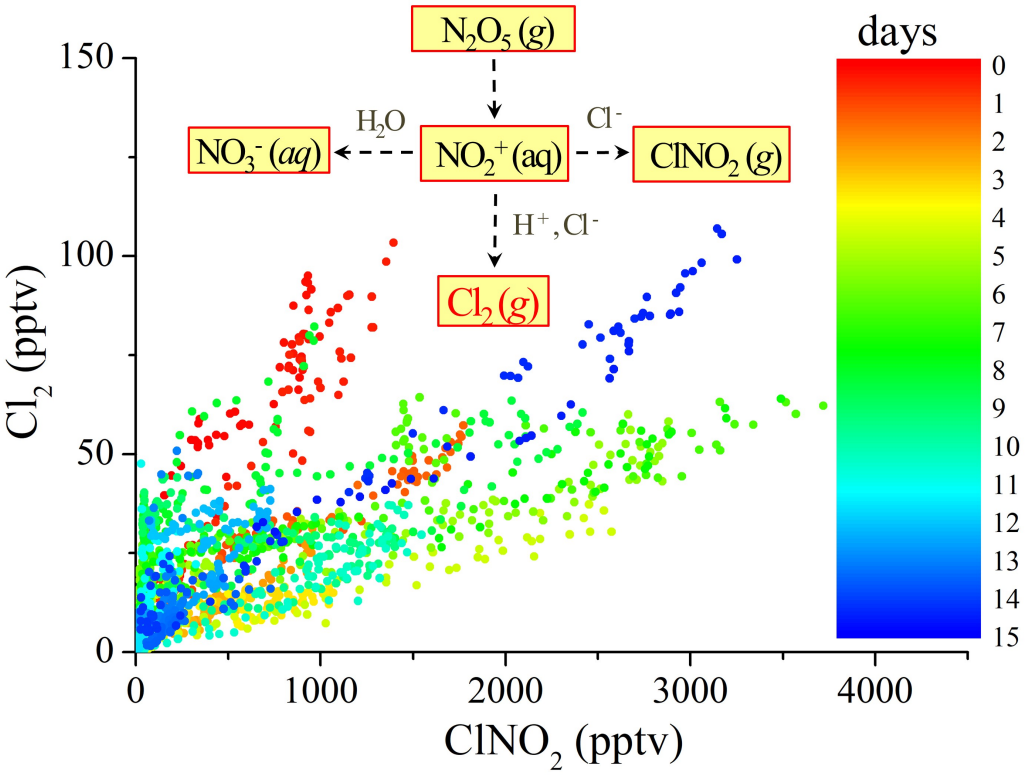

1. Introduction

Chlorine radicals ($Cl^{\cdot}$) are potent oxidizers in the atmosphere (Seinfeld and Pandis, 2016). $Cl^{\cdot}$ destroy the O_3 layer in the stratosphere, exposing the biosphere to excess ultraviolet radiation (Molina and Rowland, 1974). In the polluted troposphere, $Cl^{\cdot}$ react with volatile organic compounds (VOCs), especially alkanes, contribute to primary RO_x (= $OH+HO_2+RO_2$) production, and affect hydroxyl radical (OH) and O_3 concentrations (Simpson et al., 2015). Nitryl chloride ($ClNO_2$) is a major chlorine radical precursor in the troposphere and has been investigated around the globe over the past decade (Osthoff et al., 2008; Thornton et al., 2010; Mielke et al., 2011; Wang et al., 2016). $ClNO_2$ is an important nocturnal reservoir of chlorine and NO_x and is produced mostly at night. NO_x reacts with O_3 to form NO_3 radicals and N_2O_5 (Reactions R1 and R2). When aerosol chloride is present, $ClNO_2$ and nitrate are produced from the heterogeneous uptake of N_2O_5 on aerosols (Reaction R3) (Finlayson-Pitts et al., 1989). After sunrise, $ClNO_2$ is photolyzed to return NO_2 and release $Cl\cdot$ (Reaction R4).

$NO_2(g) + O_3(g) \rightarrow NO_3(g) + O_2(g)$ (R1)

$NO_3(g) + NO_2(g) \leftrightarrow N_2O_5(g)$ (R2)

$N_2O_5(g) + Cl^-(aq) \rightarrow ClNO_2(g) + NO_3^-(aq)$ (R3)

$ClNO_2(g) + h\nu \rightarrow Cl\cdot(g) + NO_2(g)$ (R4)

Two key kinetic parameters for quantification of $ClNO_2$ formation are $\gamma(N_2O_5)$ (i.e., N_2O_5 uptake probability on aerosols) and $\varphi(ClNO_2)$ (i.e., $ClNO_2$ production yield from N_2O_5 uptake) (Thornton et al., 2003; Behnke et al., 1997). Laboratory studies have shown that $\varphi(ClNO_2)$ is dependent on the $[Cl^-]/[H_2O]$ ratio because aqueous Cl^- and H_2O compete for the NO_2^+ intermediate, based upon which a parameterization was developed to predict $\varphi(ClNO_2)$ (hereafter denoted as $\varphi(ClNO_2)_{BT}$) (Bertram and Thornton, 2009). The parameterization was tested in several field studies, and it was found that the parameterized $\varphi(ClNO_2)$ values were significantly larger than the field-derived values (Tham et al., 2016; Wang et al., 2017; Tham et al., 2018; McDuffie et al., 2018b; Staudt et al., 2019). The exact causes of these discrepancies are not fully understood. The suppression of $\varphi(ClNO_2)$ has been observed in biomass-burning plumes in north China, but the specific species that reduced $\varphi(ClNO_2)$ were not identified (Tham et al., 2018). Some inorganic nucleophiles such as sulfate and organic nucleophiles such as acetate were recently proposed to decrease $\varphi(ClNO_2)$ by consuming NO_2^+ (McDuffie et al., 2018b; Staudt et al., 2019). Such NO_2^+-consuming nucleophiles may generate products from N_2O_5 uptake other than $ClNO_2$ and nitrate, and this is deserving of further investigation.

Besides $ClNO_2$, Cl_2 is another important chlorine radical precursor that is present in the lower troposphere (Spicer et al., 1998; Custard et al., 2016; Priestley et al., 2018). Elevated levels of Cl_2 (up to ~400 pptv) have been observed during the daytime in polar and continental environments (Liao et al., 2014; Liu et al., 2017), whereas other studies found nocturnal peaks of Cl_2 mixing ratios in polar, coastal, and continental sites (Mielke et al., 2011; Riedel et al., 2012; Riedel et al., 2013; McNamara et al., 2019). Several potential sources of Cl_2 have been proposed, such as direct emissions from power plants (Riedel et al., 2013) and water treatment facilities (Mielke et al., 2011), photochemical formation associated with O_3 (Liao et al., 2014), photoinduced production by TiO_2 (Li et al., 2020), and heterogeneous conversion from

chlorinated compounds (Reactions R5 and R6) (Deiber et al., 2004; Pratte and Rossi, 2006; McNamara et al., 2019).

$$HOCl(g) + H^+(aq) + Cl^-(aq) \rightarrow Cl_2(g) + H_2O \quad (R5)$$

$$ClONO_2(g) + H^+(aq) + Cl^-(aq) \rightarrow Cl_2(g) + HNO_3(aq) \quad (R6)$$

Cl_2 can also be produced from heterogeneous N_2O_5 uptake on acidic aerosols laden with chloride, and $ClNO_2(aq)$ has been proposed as an intermediate in Cl_2 production (Reaction R7) on the basis of laboratory studies (Roberts et al., 2008; Roberts et al., 2009). Those studies hypothesized that $ClNO_2$ first react with H^+ to form protonated $ClNO_2$ ($HClNO_2^+$), which further reacts with Cl^- to produce Cl_2 and HNO_2.

$$ClNO_2(aq) + H^+(aq) + Cl^-(aq) \rightarrow Cl_2(g) + HNO_2(aq) \quad (R7)$$

Significant correlations of $ClNO_2$ and Cl_2 were observed during an airborne campaign in the United States and were interpreted as evidence of Cl_2 production from $ClNO_2$ uptake on acidic aerosols (Haskins et al., 2019). However, this study also found that Cl_2 formation from $ClNO_2$ uptake was less efficient, because the estimated $\gamma(ClNO_2)$ value ($(2.3 \pm 1.8) \times 10^{-5}$) was two orders of magnitude lower than that suggested by laboratory studies ($(6.0 \pm 2.0) \times 10^{-3}$) (Roberts et al., 2008; Haskins et al., 2019). It remains unclear whether $ClNO_2$ uptake proceeds more slowly in ambient environments than in laboratory conditions or whether additional pathways are responsible for the formation of Cl_2. Therefore, the detailed activation process by which inert chlorine (e.g., particulate chloride) is converted to reactive chlorine remains highly uncertain and requires further research.

In April 2018, we conducted field measurements of $ClNO_2$, Cl_2, and other trace gases and aerosols in a suburban area of the Yangtze River Delta (YRD), a highly populated and industrialized region in eastern China. High levels of $ClNO_2$ with enhanced Cl_2 were observed at night. In this study, we investigated the activation of chlorine initiated by heterogeneous N_2O_5 chemistry. We first introduce prominent features of the observation results. The key parameters in $ClNO_2$ formation (i.e., $\gamma(N_2O_5)$ and $\varphi(ClNO_2)$) are then derived using the ambient data. Factors that influence $\varphi(ClNO_2)$ are discussed, with a focus on a revision of the parameterization of $\varphi(ClNO_2)$. We present observational evidence for a possible co-production

pathway of Cl_2 with $ClNO_2$ from heterogeneous reactions of N_2O_5 and propose a new parameterization for nocturnal formation of Cl_2.

2. Methods

2.1 Observation sites

The field campaign was conducted from 11 to 26 April 2018 on the Xianlin Campus of Nanjing University, which is situated in a suburban area approximately 20 km northeast of downtown Nanjing (see Fig. 1). The observation sites are surrounded by teaching and residential buildings, sparse roads, and vegetation cover for about 1 to 2 km, with no significant emission sources. Approximately 15 km northwest of the sampling sites are large-scale chemical and steel facilities, which can be sources of gaseous pollutants (CO, SO_2, NO_x, and VOCs) and particulate matters that may influence the site (Zhou et al., 2017). In addition, Shanghai is approximately 270 km southeast of the measurement site.

The main data reported in this study (i.e., N_2O_5, $ClNO_2$, and Cl_2) and the NO_x and O_3 data were obtained at the School of Atmospheric Sciences (SAS) of Nanjing University (sampling site 1). The auxiliary data, including O_3, VOCs, aerosol size distribution, and chemical composition, were obtained at the Station for Observing Regional Processes of the Earth System (SORPES, sampling site 2). Fig. 1 shows the locations of the two sampling sites. Interested readers are referred to previous studies for more information about the SORPES site (e.g., Ding et al., 2013; Sun et al., 2018; Ding et al., 2019). A comparison of O_3 measurements at the SAS and SORPES sites shows excellent agreement during the observation period (Fig. S1).

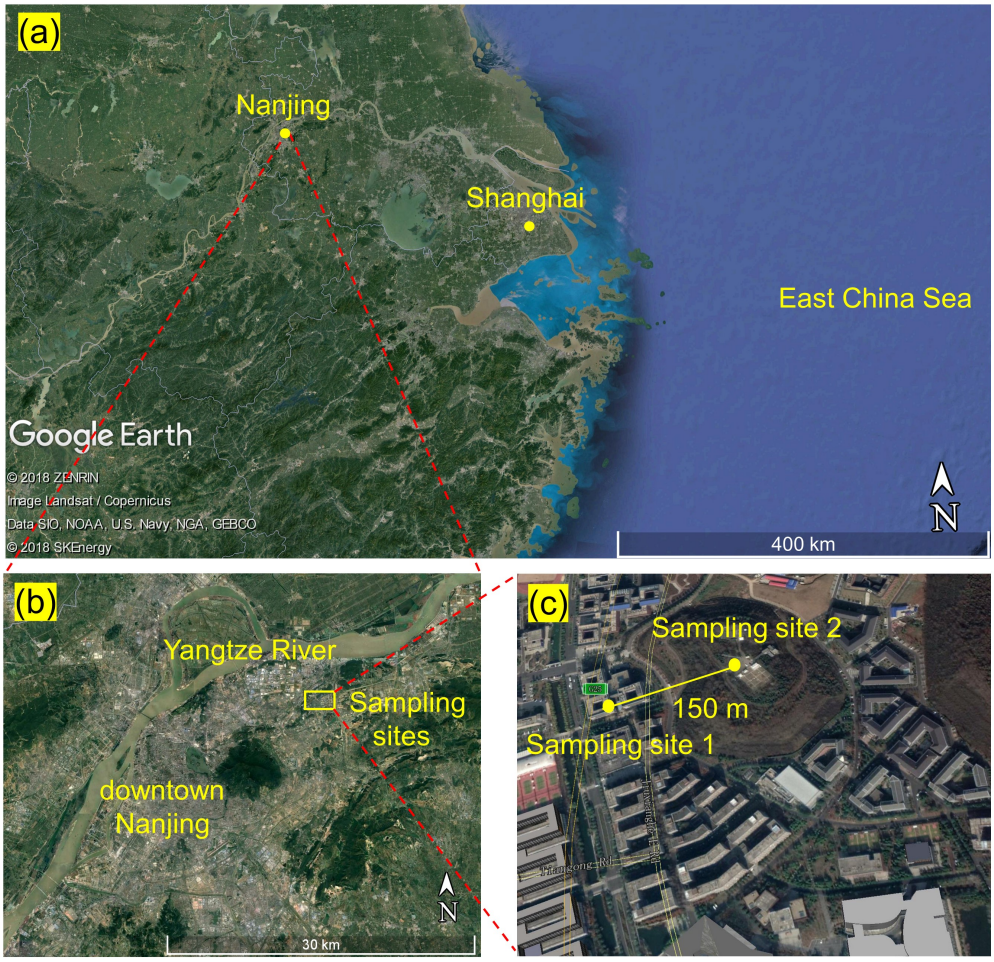

Figure 1. Sampling locations. **(a)** Location of Nanjing city in the YRD region. **(b)** Location of sampling sites in Nanjing. **(c)** Sampling sites 1 and 2 on the Xianlin campus of Nanjing University.

2.2 N_2O_5, $ClNO_2$, and Cl_2 measurements

A chemical ionization mass spectrometer coupled with a quadrupole mass analyzer (Q-CIMS, THS Instruments) was used to detect N_2O_5, $ClNO_2$, Cl_2, and HOCl. The Q-CIMS had been used in previous field campaigns to measure N_2O_5 and $ClNO_2$ (Wang et al., 2016; Tham et al., 2016). In this study, we also measured Cl_2 and HOCl and tuned the pressure of the drift tube reactor accordingly. The principles and ion chemistry of Q-CIMS were described in detail by Kercher et al. (2009). Briefly, iodide (I^-) was adopted as the primary ion for strong affinity with our target species. Charged iodide clusters, such as $IN_2O_5^-$, $ICINO_2^-$, ICl_2^-, and $IHOCl^-$, are formed by the ion molecular reactions shown in Reactions (R8) through (R11). Fig. S3 presents

an example of the CIMS spectra showing the signals of the detected species. Ion clusters with different Cl isotopes (i.e., ^{35}Cl and ^{37}Cl) were recorded to examine the identity of $ClNO_2$ and Cl_2, and this isotopic analysis confirmed that $ClNO_2$ and Cl_2 had very minor interferences (see Text S1).

$N_2O_5 + I^- \rightarrow IN_2O_5^-$ (*m/z* 235) (R8)

$ClNO_2 + I^- \rightarrow ICINO_2^-$ (*m/z* 208, 210) (R9)

$Cl_2 + I^- \rightarrow ICl_2^-$ (*m/z* 197, 199) (R10)

$HOCl + I^- \rightarrow IHOCl^-$ (*m/z* 179, 181) (R11)

The Q-CIMS was housed on the fifth floor of the SAS building. The PFA sampling tube (length, 1.5 m; outer diameter, 0.25 in) extended out through a hole in the side wall. We took precautions to minimize the deposition of particles on the inner wall of the sampling tube and tested the possible formation and loss of N_2O_5, $ClNO_2$, and Cl_2 on the sampling tube (see Text S1 for details), which showed a negligible inlet interference on the CIMS measurement. N_2O_5 and $ClNO_2$ were calibrated every two days following established methods (Wang et al., 2016). Briefly, N_2O_5 was synthesized from the reaction of NO_2 and O_3, and $ClNO_2$ was produced by passing N_2O_5 through a deliquesced NaCl slurry. The dependence of N_2O_5 sensitivity on relative humidity (RH) was tested on site (see Fig. S5) and was used to account for changes in ambient RH. A Cl_2 permeation tube was used for Cl_2 calibration (Liao et al., 2014), and the permeation rate of Cl_2 (380 ± 20 ng/m^3) was quantified by chemical titration and ultraviolet spectrophotometry (Text S4). We assumed the sensitivity of HOCl to be the same as that of ClO, and we used a sensitivity ratio of ClO to Cl_2 (0.26) that was experimentally determined by Custard et al. (2016). In this study, the HOCl data were only used qualitatively. In sum, the sensitivities of N_2O_5, $ClNO_2$, Cl_2, and HOCl were 0.42 ± 0.07, 0.35 ± 0.06, 0.86 ± 0.11, and 0.22 Hz/pptv, respectively. The detection limit (3σ) of N_2O_5, $ClNO_2$, and Cl_2 was 7 pptv, 2 pptv, and 5 pptv, respectively. The uncertainties of the N_2O_5 and $ClNO_2$ measurements were estimated to be 19% via error propagation. The Cl_2 measurement uncertainty was estimated to be 15%. The details of CIMS calibrations and uncertainty analysis are available in Text S1 and Table S3.

166

167 **2.3 Auxiliary measurements**

168 In addition to the CIMS measurement at the SAS site, meteorological factors, gaseous and
169 aerosol chemical compositions, particle size distributions, and the NO_2 photolysis frequency
170 (jNO_2) were simultaneously measured at the SORPES site (Table S1). The ionic compositions
171 of $PM_{2.5}$, including Cl^-, NO_3^-, SO_4^{2-}, and NH_4^+, were measured with an Aerosol Chemical
172 Speciation Monitor (ACSM, Aerodyne Research Inc.) and MARGA (Metrohm, Switzerland).
173 The hourly-averaged ionic compositions from ACSM and MARGA showed good agreement
174 (see Fig. S6). In addition, HNO_3 was also measured by MARGA. In this study, the 10-min
175 averaged ACSM data, including total organics, were used for subsequent analysis. The mass
176 concentration of H^+ ($\mu g/m^3$) was estimated to achieve electric charge balance of the cation
177 (NH_4^+) and anions (Cl^-, NO_3^-, and SO_4^{2-}) of the ACSM data. The molar concentrations of
178 inorganic ions (i.e., [Cl^-], [NO_3^-], [SO_4^{2-}], [NH_4^+], and [H^+]) and total organics ([Org]) were
179 estimated using the extended aerosol inorganics model (E-AIM, model III) (Wexler, 2002). The
180 molecular weight of the organic molecules was assumed to be 250 g/mol (McDuffie et al.,
181 2018b). The dry-state submicron particle size distribution was measured with a Scanning
182 Mobility Particle Sizer (SMPS, TSI Inc.), and the data were used to estimate the aerosol surface
183 area density (S_a) with the assumption of spherical particles. The hygroscopic growth factor of
184 the particle size was based on an empirical parameterization, $GF = 0.582\left(8.46 + \frac{1}{1 - RH}\right)^{1/3}$
185 (Lewis, 2008). The VOCs were measured with a proton transfer reaction time-of-flight mass
186 spectrometer (PTR-TOF-MS, Ionicon).

187

188 **2.4 Production and loss of NO_3 and N_2O_5**

189 NO_3 radicals are primarily produced from NO_2 and O_3 (Reaction R1). The production rate
190 equation of NO_3 ($P(NO_3)$) is shown as follows (Eq. (1):

191 $$P(NO_3) = k_1[NO_2][O_3] \quad (1)$$

192 where k_1 is the rate constant of Reaction R1. NO_3 is mainly removed by gas-phase reactions
193 with VOCs and NO (Eq. (2)) and heterogeneous loss via N_2O_5 uptake (Eq. (3)), where $k(NO_3)$

and $k(N_2O_5)$ are the first-order loss rate coefficients of NO_3 and N_2O_5, respectively.

$$k(NO_3) = k_{NO+NO_3}[NO] + \sum k_i[VOC_i] \quad (2)$$

$$k(N_2O_5) = \frac{1}{4}c(N_2O_5)S_a\gamma(N_2O_5) \quad (3)$$

where k_{NO+NO_3} and k_i denote the reaction rate constants of NO_3 with NO and VOC, respectively, and $c(N_2O_5)$ is the average velocity of N_2O_5 molecules. Other minor loss pathways of NO_3 and N_2O_5 were not considered (e.g., homogeneous loss of N_2O_5).

2.5 Estimation of $\varphi(ClNO_2)$ and $\gamma(N_2O_5)$

$\varphi(ClNO_2)$ and $\gamma(N_2O_5)$ were estimated using the observation data and parameterization. We used the observed increasing rates of $ClNO_2$ and total nitrate (i.e., HNO_3+NO_3^-) to derive the values for $\gamma(N_2O_5)$ and $\varphi(ClNO_2)$ in the selected cases (Phillips et al., 2016). Details of the method are described elsewhere (Tham et al., 2016; Phillips et al., 2016). Briefly, the production rate of $ClNO_2$ ($P(ClNO_2)$) is calculated as follows (Eq. (4)).

$$P(ClNO_2) = \frac{1}{4}c(N_2O_5)S_a\gamma(N_2O_5)[N_2O_5]\varphi(ClNO_2) \quad (4)$$

The production rate of total nitrate induced by N_2O_5 uptake during the night ($P(NO_3^-)$) is shown by Eq. (5).

$$P(NO_3^-) = \frac{1}{4}c(N_2O_5)\ S_a\gamma(N_2O_5)[N_2O_5](2-\varphi(ClNO_2)) \quad (5)$$

$\varphi(ClNO_2)$ is obtained by combining Eqs. (4) and (5).

$$\varphi(ClNO_2) = 2\left(1+\frac{P(NO_3^-)}{P(ClNO_2)}\right)^{-1} \quad (6)$$

And $\gamma(N_2O_5)$ is derived as follows (Eq. (7)).

$$\gamma(N_2O_5) = \frac{2(P(ClNO_2) + P(NO_3^-))}{c(N_2O_5)S_a[N_2O_5]} \quad (7)$$

This method assumes that: (1) air masses are relatively stable; and (2) N_2O_5 uptake dominates NO_3^- production at night (Tham et al., 2018). Assumption (1) requires careful selection of the cases of interest. Regarding assumption (2), major nocturnal production pathways of total nitrate should be evaluated, such as comparing the reaction rate of N_2O_5 heterogeneous loss ($k(N_2O_5)$*$[N_2O_5]$) with that of NO_3 + VOC ($k(NO_3)$*$[NO_3]$), which may produce HNO_3 via H-abstraction reactions.

$\varphi(ClNO_2)$ was also calculated with the parameterization shown in Eq. (8), in which the k_4/k_3 ratio was adopted as 483 ± 175 (Bertram and Thornton, 2009).

$$\varphi(ClNO_2)_{BT} = \left(1 + \frac{[H_2O]}{k_4/k_3[Cl^-]}\right)^{-1} \quad (8)$$

When considering the potential competitive effect of other species (denoted as "Y^-"), such as sulfate or aerosol organics, for the NO_2^+ intermediate, the following equation (Eq. (9)) was established (McDuffie et al., 2018b). Rearrangement of Eq. (9) yields Eq. (10), in which plotting $\left(\frac{1}{\varphi(ClNO_2)} - 1\right) * \frac{[Cl^-]}{[H_2O]}$ to $\frac{[Y^-]}{[Cl^-]}$ should exhibit a positive correlation. k_5 represents a constant reaction rate coefficient of "Y^-" with NO_2^+.

$$\varphi(ClNO_2) = \frac{1}{1 + \frac{k_3[H_2O]}{k_4[Cl^-]} + \frac{k_5[Y^-]}{k_4[Cl^-]}} \quad (9)$$

$$\left(\frac{1}{\varphi(ClNO_2)} - 1\right) * \frac{[Cl^-]}{[H_2O]} = \frac{k_3}{k_4} + \frac{k_5[Y^-]}{k_4[Cl^-]} \quad (10)$$

3. Results and Discussions

3.1 Overall observation results

Fig. 2 depicts the time series of N_2O_5, $ClNO_2$, Cl_2, and related species. Overall, the observation sites experienced moderate levels of pollution during the study period ($PM_{2.5}$, 44.8 ± 18.3 μg/m^3; CO, 0.4 ± 0.2 ppmv; SO_2, 3.1 ± 1.8 ppbv; NO_x, 18.1 ± 16.6 ppbv; O_3, 25.8 ± 18.4 ppbv). The on-site observations indicated mostly stagnant weather with low wind speeds (1 m/s in average). No precipitation was observed except for the evening of 13 April from 22:00 to 22:30 local time. The nocturnal NO mixing ratios were usually near the detection limit of the NO instrument, and the presence of abundant NO_2 and O_3 favored N_2O_5 formation and subsequent heterogeneous processes.

The most salient features of the observation were the high levels of $ClNO_2$ and moderate levels of Cl_2 that were present during the night. The $ClNO_2$ mixing ratios exceeded 1 ppbv on 12 of the 15 nights. The observed $ClNO_2$ levels were among the highest in the world, with a peak mixing ratio (1-min average, 3.7 ppbv) slightly higher than that of north China (1-min average, 2.1 ppbv) (Tham et al., 2016) but lower than that reported in south China (1 min

247 average, 8.3 ppbv) (Yun et al., 2018). The frequent occurrence of high $ClNO_2$ levels was favored
248 by several factors, including elevated levels of N_2O_5 (1 ppbv), humid weather (RH, 67.7 ±
249 20.7 %), and chloride availability (0.36 ± 0.31 μg/m^3) during the field campaign. When high
250 levels of $ClNO_2$ were observed, elevated concentrations of particulate nitrate as high as 40.8
251 μg/m^3 (10-min average) were also present. We noticed that $ClNO_2$ and particulate nitrate
252 concentrations both increased more rapidly after midnight than before midnight from 15 to 19
253 April, which is discussed further below.

254 Moderate levels of Cl_2 (up to 100 pptv) were also observed during the night. Cl_2 mixing ratios
255 exhibited a clear diurnal pattern, peaking at night and decreasing during the day due to
256 photolysis. The nocturnal peaks of Cl_2 mixing ratios showed discrepancies from some previous
257 observations in which an elevated level of Cl_2 was found during the day (Liao et al., 2014; Liu
258 et al., 2017). The Cl_2 and $ClNO_2$ mixing ratios reached peaks synchronously during most nights,
259 and both species decreased in abundance or were absent in NO-rich plumes (e.g., the nights of
260 13 and 25 April), which suggests that Cl_2 and $ClNO_2$ were produced from common sources.
261 Similar nighttime correlations of Cl_2 and $ClNO_2$ were also observed in the United States and in
262 northern China (Qiu et al., 2019; Haskins et al., 2019). A subsequent analysis of the present
263 study aims to elucidate the nighttime formation processes of $ClNO_2$ and Cl_2.

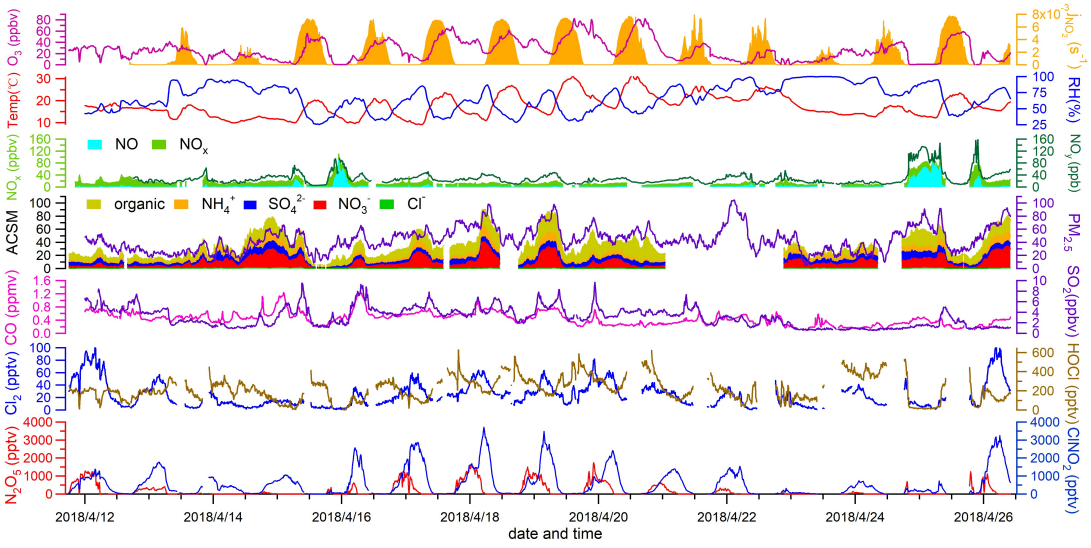

264

265 **Figure 2.** Time series of $ClNO_2$, Cl_2, and related measurements during field observations from
266 11 to 26 April 2018. Data gaps were caused by technical problems or calibrations.
267

3.2 High $ClNO_2$ cases

Fig. 3 shows the observation results from 17 and 18 April to further illustrate the $ClNO_2$ formation process. This case had the highest $ClNO_2$ observed during the campaign and shows an example of high $ClNO_2$ mixing ratios after midnight. As shown in Fig. 3a, the mixing ratio of $ClNO_2$ began to increase after sunset (18:00 17 April) and decreased after midnight. The period between 22:00 and 24:00 on 17 April was noted as plume 1. After midnight, the $ClNO_2$ mixing ratios exhibited a more rapid increase from 03:00 to 05:00 on 18 April (plume 3), and the particulate nitrate concentration also synchronously and significantly increased. Plumes 1 and 3 were identified as being different, resulting from an air mass shift between 00:00 and 03:00 on 18 April (plume 2), as indicated by abrupt changes in the RH, temperature, and O_3. We compared the backward trajectories from plume 1 to plume 3 and found no significant difference (figures not shown here). Thus, the change in the air mass from plume 1 to plume 3 was likely a local phenomenon.

The $P(NO_3)$ and NO_3 loss pathways during plumes 1 and 3 were calculated and compared in Fig. 3b-d using the methods described in Section 2.4. The $P(NO_3)$ was slightly lower during plume 3 than during plume 1, and a larger proportion of NO_3 was lost via the N_2O_5 hydrolysis pathway in plume 3. Thus, the air mass shift, in addition to the higher rate of N_2O_5 hydrolysis, was responsible for the elevated $ClNO_2$ levels observed after midnight.

Compared with the high levels of $ClNO_2$ (up to 3.5 ppbv) on the night of 17 April, the concentration of Cl^- was low and relatively constant (~0.1 ppbv) during that period. The low chloride but high $ClNO_2$ levels were also observed in previous studies, and HCl partition was proposed to replenish particulate chloride to sustain the $ClNO_2$ production (Osthoff et al., 2008; Thornton et al., 2010).

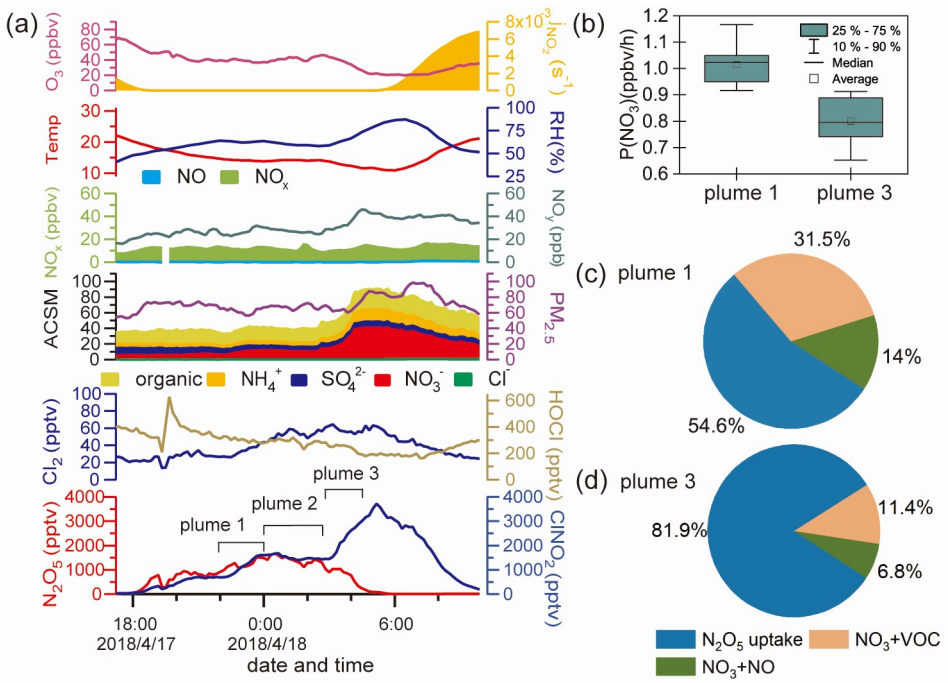

Figure 3. Detailed analysis of a high $ClNO_2$ episode observed on 17–18 April. **(a)** Time series of $ClNO_2$ and related species. **(b)**, **(c)**, and **(d)** Comparisons of $P(NO_3)$ and NO_3 loss pathways in plumes 1 and 3.

3.3 $ClNO_2$ production yield from N_2O_5 uptake

$\varphi(ClNO_2)$ was estimated to investigate its influencing factors and the performance of parameterization in selected cases. The methods described in Section 2.5 were used to estimate the $\varphi(ClNO_2)$ and $\gamma(N_2O_5)$ using the observation data. As these methods assume a stable air mass and the dominance of N_2O_5 uptake in nitrate formation, we applied the following criteria when selecting cases for this analysis. First, the NO mixing ratios must be less than 0.1 ppbv. When significant levels of NO were present, the N_2O_5 chemistry was suppressed. Second, primary pollutants such as CO, SO_2, and meteorological factors (wind, temperature, and RH) were required to exhibit relatively constant levels or stable trends within the cases. Third, the $ClNO_2$ and nitrate levels had to be correlated ($R^2 > 0.6$) and show increasing trends. Fifteen cases that lasted 30 min to 3 hours were selected, and 10-min averaged data were used for calculation. Fig. S7 shows an example of this calculation, which corresponds to plume 1 on 17 April (Fig. 3). We then evaluated the loss pathways of NO_3 in the fifteen cases. The results show that the NO_3 + VOCs reactions contributed less than one third of the total NO_3 + N_2O_5 loss (e.g.,

310 Fig. 3c, d). Nocturnal total nitrate production was thus dominated by N_2O_5 uptake, and only a
311 small proportion of nitrate was produced by NO_3+VOCs reactions.

312 The derived $\gamma(N_2O_5)$ values ranged from 0.004 to 0.014 (mean, 0.008 ± 0.004). The highest
313 $\gamma(N_2O_5)$ values (0.0135 and 0.0139) were derived between 03:00 and 05:00 on 18 April (i.e.,
314 plume 3 in Fig. 3), which was consistent with the rapid increase in $ClNO_2$ mixing ratios during
315 that period. The variations in the $\gamma(N_2O_5)$ value depended mainly on $[H_2O]$ ($R^2 = 0.49$) (see Fig.
316 S8) but showed little correlation with other influencing factors, such as $[Cl^-]$, $[NO_3^-]$, and V_a/S_a
317 (figures not shown here). The dominant influence of $[H_2O]$ on the $\gamma(N_2O_5)$ value was also
318 reported in previous studies (e.g., Tham et al., 2018).

319 The $\varphi(ClNO_2)$ value ranged from 0.28 to 0.89 (mean, 0.56 ± 0.15). The $\varphi(ClNO_2)$ value
320 exhibited an obvious nonlinear relationship with the $[Cl^-]/[H_2O]$ ratio ($R^2 = 0.52$) (Fig. 4a),
321 which is consistent with previous laboratory results (Bertram and Thornton, 2009). However,
322 current parameterization of $\varphi(ClNO_2)$ based on $[Cl^-]/[H_2O]$ ($\varphi(ClNO_2)_{BT}$) tended to
323 overestimate the observed $\varphi(ClNO_2)$ value (Fig. 4b).

324 Here we give two explanations for the inconsistency between the $\varphi(ClNO_2)_{BT}$ and the field-
325 derived $\varphi(ClNO_2)$. First, the reactivity of chloride with NO_2^+ (i.e., k_4/k_3 in Eq. 8) was reduced
326 in ambient environments due to complicated issues of the mixing state, phase state, and activity
327 coefficient. As $\varphi(ClNO_2)$ is positively dependent upon $[Cl^-]$, a reduction in chloride reactivity
328 could decrease the $\varphi(ClNO_2)$ value in ambient particles. This explanation is supported by
329 previous studies of $\gamma(N_2O_5)$ (Morgan et al., 2015; McDuffie et al., 2018a), which showed that
330 when the enhancement effect of chloride on $\gamma(N_2O_5)$ was neglected, the parameterized $\gamma(N_2O_5)$
331 better matched the observed $\gamma(N_2O_5)$. The second explanation deals with other unknown factors
332 that reduce the $\varphi(ClNO_2)$ value. The parameterization $\varphi(ClNO_2)_{BT}$ only considered the
333 $[Cl^-]/[H_2O]$ ratio, not other aqueous species that could suppress $\varphi(ClNO_2)$, leading to the
334 overestimation of $\varphi(ClNO_2)_{BT}$ values.

335 Regarding the second explanation, we examined the possibility of sulfate and aerosol
336 organics competing with $[Cl^-]$ for the NO_2^+ intermediate (see Section 2.4 and Eq. (10)). The
337 statistical results show that aerosol organics could reduce $\varphi(ClNO_2)$ values ($R^2 = 0.41$; Fig. S9b),

but sulfate did not show such an influence (R^2 = 0.08; Fig. S9a). The latter result contrasts with the finding of a recent laboratory study, which indicated that both sulfate and some organics (e.g., carboxylate) suppress $ClNO_2$ formation (Staudt et al., 2019).

By incorporating the suppression effect of aerosol organics, we performed regressions of $\varphi(ClNO_2)$ and obtained an improved parameterization of $\varphi(ClNO_2)$ (noted as $\varphi(ClNO_2)_{BT+Org}$). The parameterized $\varphi(ClNO_2)_{BT+Org}$ better matches the observed $\varphi(ClNO_2)$ at low to median yields (0~0.75) and the R^2 and slope values in the linear regression are closer to 1 (Fig. 4b). However, the parameterized $\varphi(ClNO_2)_{BT+Org}$ is smaller than the observed $\varphi(ClNO_2)$ at high yields (0.75~0.9), which may be attributable to other unconstrained factors in the parameterization, e.g., mixing state and phase state issues. In Eq. (11), the factor 483 (k_4/k_3 in Eq. 9) was adopted from (Bertram and Thornton, 2009), and the factor 235 (k_4/k_5 in Eq. 9) was derived here by iterative algorithms to achieve the least-square errors between the observed and parameterized $\varphi(ClNO_2)$ values. Here we assumed that the observed aerosol organics were all water-soluble and reactive toward NO_2^+, as previous studies did (McDuffie et al., 2018a; McDuffie et al., 2018b). The unknown water-soluble proportion of aerosol organics is factored in k_5. Given that k_4/k_3 = 483 and k_4/k_5 = 235, k_5/k_3 was calculated as 2.06, which suggests that the reaction rate constant of aerosol organics with NO_2^+ was twice that of the H_2O + NO_2^+ reaction. A recent laboratory study (Staudt et al., 2019) derived k_5/k_3 = 3.7 for acetate, which happens to be similar to the value derived for ambient aerosol at our site.

$$\varphi(ClNO_2)_{BT+Org} = \left(1+\frac{[H_2O]}{483[Cl^-]}+\frac{[Org]}{235[Cl^-]}\right)^{-1} \quad (11)$$

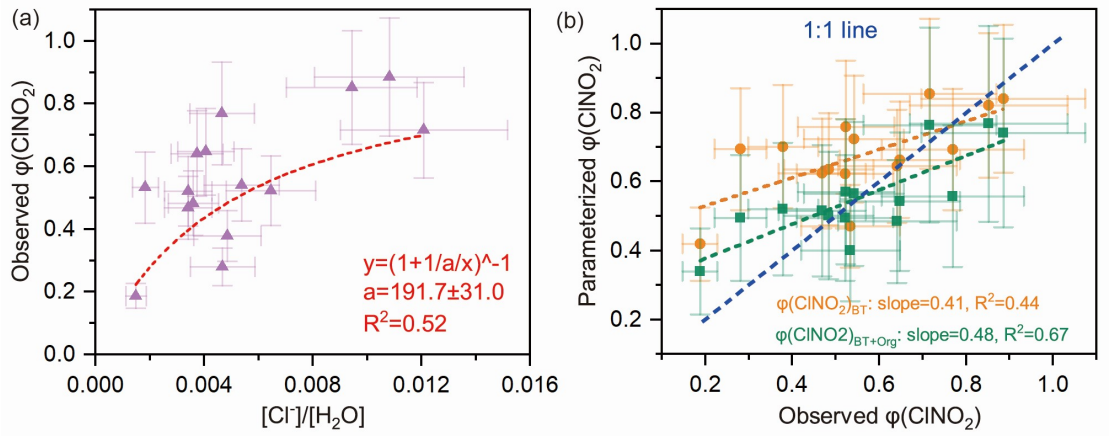

Figure 4. Influencing factors and parameterizations of $\varphi(ClNO_2)$. **(a)** Dependence of $\varphi(ClNO_2)$

on the $[Cl^-]/[H_2O]$ ratio. Dashed red line shows nonlinear fitting of $\varphi(ClNO_2)$; "a" represents the k_4/k_3 in Eq. (8). **(b)** Comparison of parameterized $\varphi(ClNO_2)$ and observed $\varphi(ClNO_2)$, where $\varphi(ClNO_2)_{BT}$ denotes the parameterization proposed by Bertram and Thornton (2009), and $\varphi(ClNO_2)_{BT+Org}$ represents the revised parameterization used in this study (see Eq. (11)).

3.4 Nocturnal Cl_2 formation

3.4.1 Cl_2 as a co-product of $ClNO_2$ from N_2O_5 uptake

To elucidate the formation pathways of the elevated levels of Cl_2 observed during the night, we investigated the correlations of Cl_2 with the $ClNO_2$, HOCl, and SO_2 and the diurnal variations of these species (Fig. 5a–5d). Our result suggests that Cl_2 was related to $ClNO_2$, but the HOCl pathway (R5) and coal burning were of minor importance at our site. $ClONO_2$ was not measured during our study. Recent field measurements at a rural site in northern China reported low $ClONO_2$ levels at night (maximum ~ 15 pptv) (Breton et al., 2018). We believe that the $ClONO_2$ levels at our site were also low, and production pathway (R6) was insignificant given low $\gamma(ClONO_2)$ ($\sim 10^{-3}$) (Haskins et al., 2019). At our site, the $Cl_2/ClNO_2$ ratios varied on different nights, which implies that differences exist in the production efficiencies of Cl_2 relative to those of $ClNO_2$.

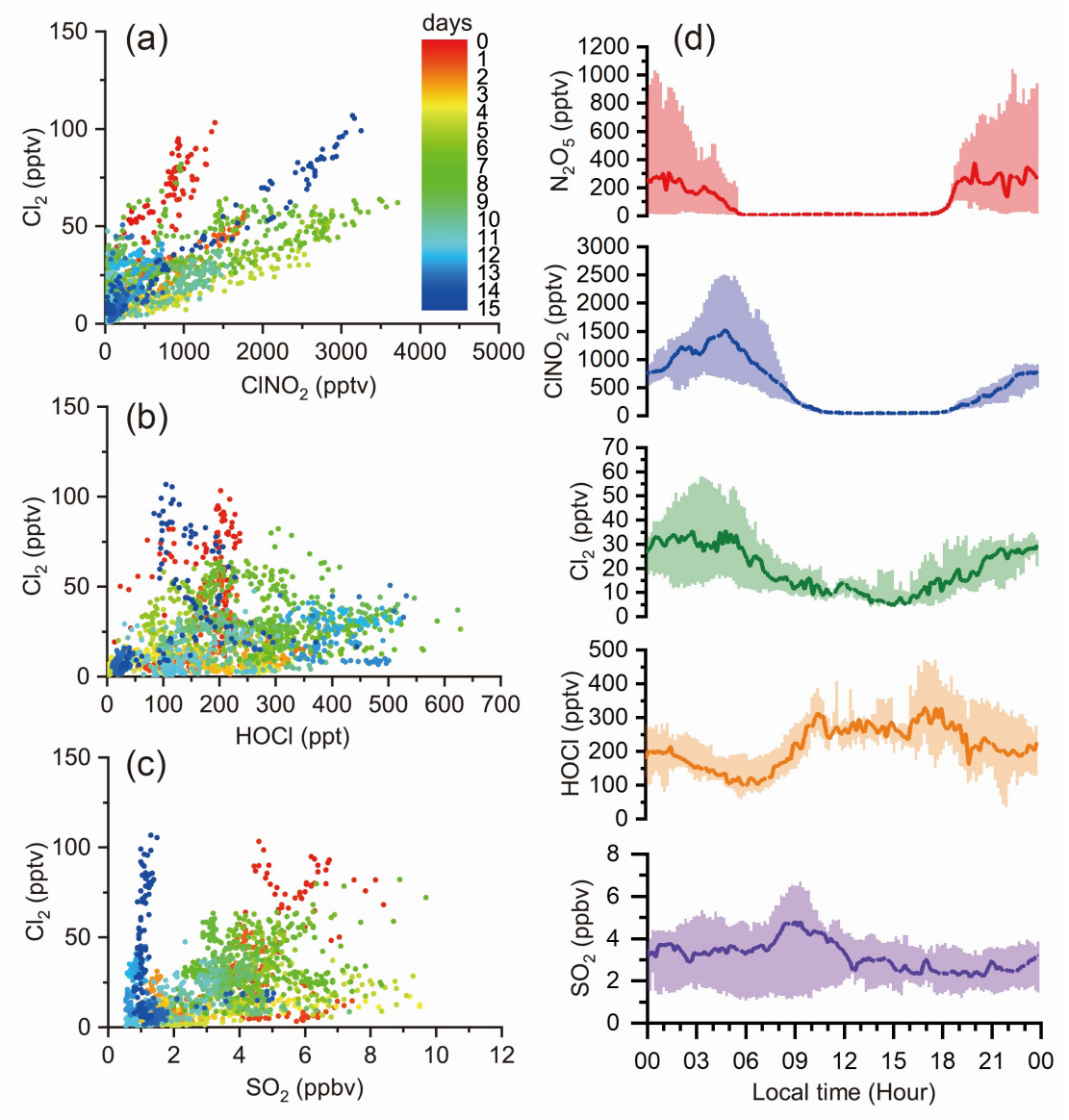

Figure 5. Correlations among Cl_2, $ClNO_2$, HOCl, and SO_2 and their diurnal profiles **(a)**, **(b),** and **(c)** show the correlations of Cl_2 with $ClNO_2$, HOCl, and SO_2 respectively, during the whole campaign. Dots represent 10-min averaged values colored according to campaign days. **(d)** exhibits the diurnal variation of Cl_2, $ClNO_2$, HOCl, and SO_2.

The current mainstream interpretation of the observed correlation of $ClNO_2$ and Cl_2 is that Cl_2 is produced from $ClNO_2$ uptake (Ammann et al., 2013; Qiu et al., 2019; Wang et al., 2019; Haskins et al., 2019). We provide evidence that this interpretation does not apply to measurements from our site. We assessed the $ClNO_2$ uptake hypothesis by examining the magnitude of $\gamma(ClNO_2)$ needed to explain the nocturnal increase in Cl_2 mixing ratios and the

dependence of $\gamma(ClNO_2)$ on its known influencing factors. Assuming a unity yield of Cl_2 from $ClNO_2$ uptake, the increasing rate of Cl_2 mixing ratios was calculated with Eq. (12). Eq. (13), which was derived by rearrangement of Eq. (12), was adopted to estimate $\gamma(ClNO_2)$ via the observed Cl_2 and $ClNO_2$ levels.

$$d[Cl_2]/dt = \frac{1}{4}c(ClNO_2)S_a\gamma(ClNO_2)[ClNO_2] \quad (12)$$

$$\gamma(ClNO_2)_{obs} = \frac{4d[Cl_2]/dt}{c(ClNO_2)S_a[ClNO_2]} \quad (13)$$

where $c(ClNO_2)$ is the mean molecular velocity of $ClNO_2$ (m/s), and $[ClNO_2]$ represents the averaged ambient concentration of $ClNO_2$ in the cases of interest.

$\gamma(ClNO_2)_{obs}$ was estimated in the selected cases following criteria 1 and 2 in Section 3.3, and a steady increase in Cl_2 mixing ratios was required. The resulting values of $\gamma(ClNO_2)_{obs}$ were compiled according to the local time and are presented in box charts (Fig. 6a). Fig. 6a also shows the potential factors influencing $\gamma(ClNO_2)$: $[Cl^-]$, $[H^+]$, and particle diameters (D_p). Here, D_p was an influencing factor of $\gamma(ClNO_2)$ because $ClNO_2$ uptake was regarded as a volume-limited mechanism (Ammann et al., 2013; Haskins et al., 2019). $[H^+]$ and $[Cl^-]$ was considered because the previous laboratory study proposed that H^+ and Cl^- were reactants in Cl_2 production (Roberts et al., 2008). Positive correlations of $\gamma(ClNO_2)$ with $[Cl^-]$ and D_p were also found in a field study (Haskins et al., 2019). Each box represents the $\gamma(ClNO_2)$, $[Cl^-]$, $[H^+]$, or D_p of 10-min resolutions derived on individual days. For example, the box for 18:00–19:00 contains the $\gamma(ClNO_2)$ estimated at 18:00–19:00 on 11, 12, and 14 April (Fig. 6b–6d, orange lines). Fig. 6b–6d displays the observed Cl_2 levels (blue lines) and the projected trends of Cl_2 levels from Eq. (12), where the grey lines adopted the highest $\gamma(ClNO_2)$ value, 6.69×10^{-5} observed in the field study of Haskins et al. (2019). During early evening hours (i.e., 18:00–19:00), the $\gamma(ClNO_2)$ value derived in our study was one to two orders of magnitude higher than those in that study. This result implies that either $ClNO_2$ uptake was much faster at our site or other pathways were involved in Cl_2 production. We provide evidence below that the latter is likely the case.

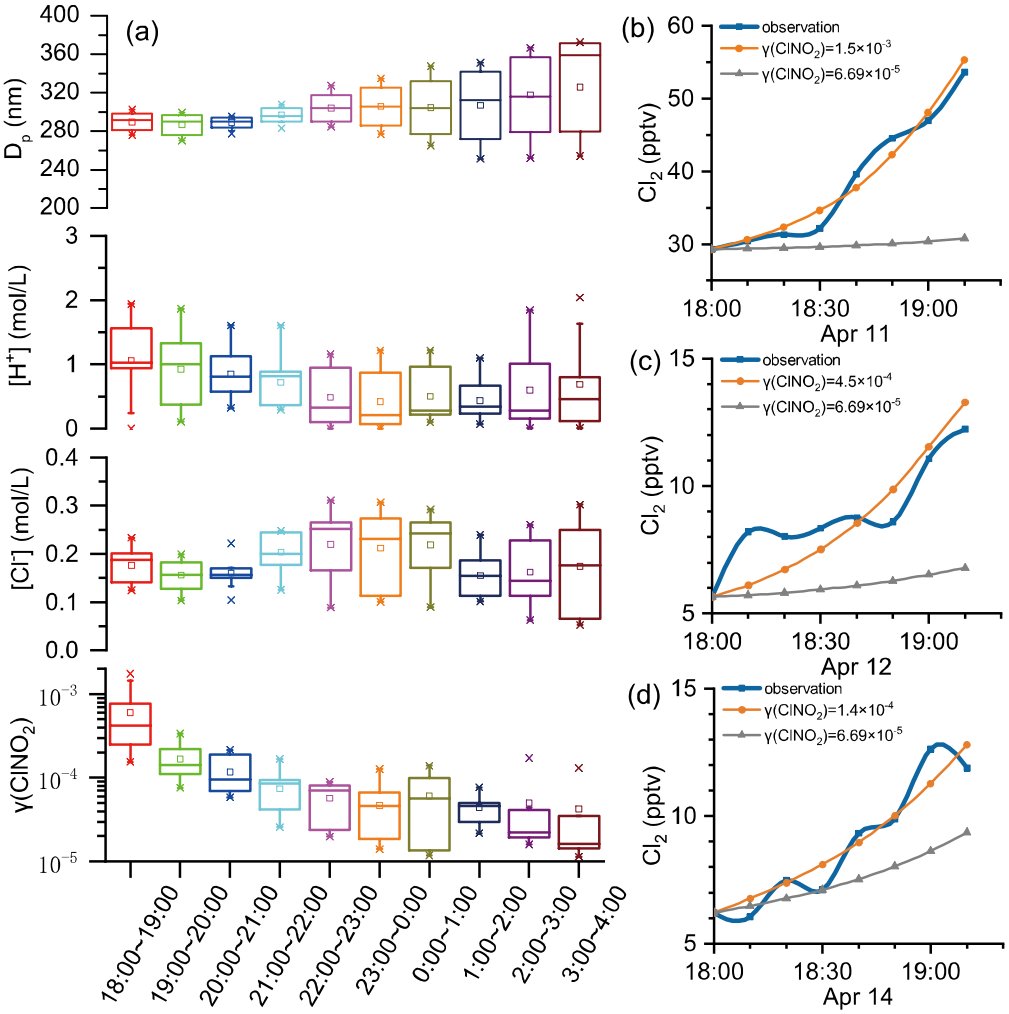

Figure 6. $\gamma(ClNO_2)$ estimated using field observation data. **(a)** $\gamma(ClNO_2)_{obs}$, $[Cl^-]$, $[H^+]$, and D_p estimated at various nighttime periods. **(b)–(d)** Trends of increasing trends of Cl_2 mixing ratios during the early evening hours on 11, 12, and 14 April, respectively. Orange and gray lines represent the projected trend of Cl_2 mixing ratios using Eq. (12) with constant $\gamma(ClNO_2)$ values and observed $ClNO_2$ levels.

If the $ClNO_2$ uptake is the main production channel for Cl_2, we would expect to see positive correlations between $\gamma(ClNO_2)$ and factors such as $[Cl^-]$, $[H^+]$, and D_p, according to previous laboratory and field studies (Roberts et al., 2008; Haskins et al., 2019). At our site, as the increasing rate of Cl_2 concentrations ($d[Cl_2]/dt$) did not change significantly during the night (Fig. 5d), the $\gamma(ClNO_2)$ value was constrained by a sharp decreasing trend to compensate for the increasing $ClNO_2$ levels after dusk (see Eq. 12). The highest $\gamma(ClNO_2)_{obs}$ value determined

during the early evening hours (18:00–19:00) was similar to the laboratory-derived $\gamma(ClNO_2)_{obs}$ value on acidic salt films (6×10^{-3}) (Roberts et al., 2008). However, the lowest $\gamma(ClNO_2)_{obs}$ value estimated during later nighttime hours (22:00–04:00) was two orders of magnitude lower (10^{-5}). The large variations in the $\gamma(ClNO_2)$ value contrasted with the relatively stable levels of $[Cl^-]$, $[H^+]$, and D_p at various times of night, which is in opposition to the current understanding of the relationship between the $\gamma(ClNO_2)$ and these factors. In our study, the D_p was derived from the ratio of wet V_a to S_a by assuming volume-limited uptake (Ammann et al., 2013). We also calculated D_p assuming surface-limited uptake (diameter of the average surface area), and no correlation with $\gamma(ClNO_2)_{obs}$ was indicated. Moreover, the $\gamma(ClNO_2)_{obs}$ showed no obvious relationship with other factors such as T, RH, aerosol liquid water content (ALW), NO_3^-, SO_4^{2-}, NH_4^+, and aerosol organics (figure not shown). To sum up, the $ClNO_2$ uptake pathway alone cannot explain the nocturnal increase in Cl_2 mixing ratios that we observed at our study site.

We propose another hypothesis to explain the $ClNO_2$–Cl_2 correlation and suggest that Cl_2 is a co-product with $ClNO_2$ produced from N_2O_5 uptake, in which $ClNO_2$ is not necessarily an intermediate of Cl_2 production. The mechanism is depicted in Figure 7 and goes as follows. It is known that N_2O_5 hydrolysis on aerosol is responsible for the production of NO_2^+. According to the hybrid orbital theory, the NO_2^+ ion has two non-bonded π molecular orbitals due to participation of the d orbital of the central nitrogen atom (Baird and Tayler, 1981). $ClNO_2$ is formed via the nucleophilic addition of Cl^- to one of the π molecular orbitals of NO_2^+ (Figure 7a) (Taylor, 1990; Behnke et al., 1997). In the same way, we propose a side reaction that the second Cl^- can attach to the other π molecular orbital of NO_2^+ and form a short-lived HNO_2Cl_2 intermediate in presence of H^+. It is proposed that the unstable HNO_2Cl_2 decomposes to produce Cl_2 (and HONO) (Figure 7b). This mechanism can explain concurrent productions of Cl_2 and $ClNO_2$ from N_2O_5 hydrolysis but needs confirmation by additional laboratory and theoretical studies.

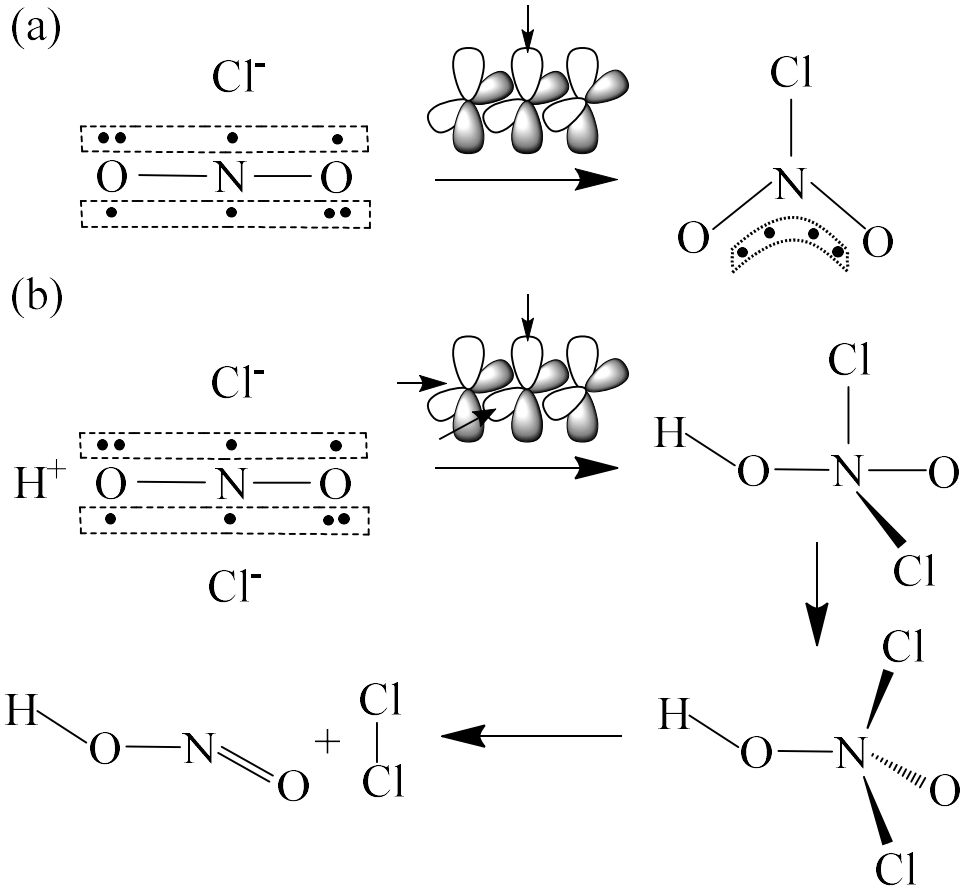

Figure 7. Proposed formation mechanisms of $ClNO_2$ and Cl_2 from N_2O_5 uptake. **(a)** production of $ClNO_2$ from NO_2^+ and Cl^-. **(b)** production of Cl_2 from NO_2^+, Cl^-, and H^+.

3.4.2 Parameterizing Cl_2 formation from N_2O_5 uptake

We propose a new framework to estimate nighttime Cl_2 production by treating Cl_2, $ClNO_2$, and most nitrate all ultimately originating from N_2O_5 uptake. We assign a production yield to Cl_2 from the N_2O_5 uptake ($\varphi(Cl_2)$) analogous to the $ClNO_2$ yield and calculate this metric using Eq. (14):

$$\varphi(Cl_2) = \frac{d[Cl_2]/dt}{k(N_2O_5)[N_2O_5]} \quad (14)$$

The above formulation does not rule out the production of Cl_2 from the $ClNO_2$ uptake, because such production, if any, is also a result of N_2O_5 uptake and has thus been incorporated in Eq. (14). We calculated $\varphi(Cl_2)$ in the same cases in which $\gamma(N_2O_5)$ and $\varphi(ClNO_2)$ were derived, because the availability of $\gamma(N_2O_5)$ was a prerequisite of deriving $\varphi(Cl_2)$. The estimated $\varphi(Cl_2)$

value was 0.01–0.04 (Table S2). The dependences of $\varphi(Cl_2)$ on its potential influencing factors (i.e., $[Cl^-]$, $[H^+]$, and D_p) were examined. The results show that $\varphi(Cl_2)$ had positive correlations with both $[Cl^-]$ (R^2 = 0.74) and $[H^+]$ (R^2 = 0.75) and that the data had a high $\varphi(Cl_2)$ region and a low $\varphi(Cl_2)$ region (Fig. 8a, b). The low $\varphi(Cl_2)$ values were found in continental air masses with relatively lower chloride concentrations, more alkaline ammonium, less acidic sulfate and nitrate, and thus lower acidity (Fig. 8d). In contrast, the high $\varphi(Cl_2)$ values were associated with marine air masses with higher loadings of aerosol chloride, less ammonium, and more acidic compounds, and thus higher acidity (Fig. 8c). The higher acidity in the marine air masses may be explained by their passage over the industrialized cities in the YRD where large amount of SO_2 and NO_x are emitted. The average concentrations of SO_2 (3.9 ± 0.1 ppbv) and NO_x (13.1 ± 3.1 ppbv) in the marine air masses were higher than those (NO_x: 11.5 ± 0.6 ppbv, SO_2: 3.3 ± 0.3 ppbv) in the inland air masses. The dependences of the defined $\varphi(Cl_2)$ on $[Cl^-]$ and $[H^+]$ indicate that nocturnal Cl_2 production requires the presence of highly acidic chloride-rich particles and sufficient levels of N_2O_5.

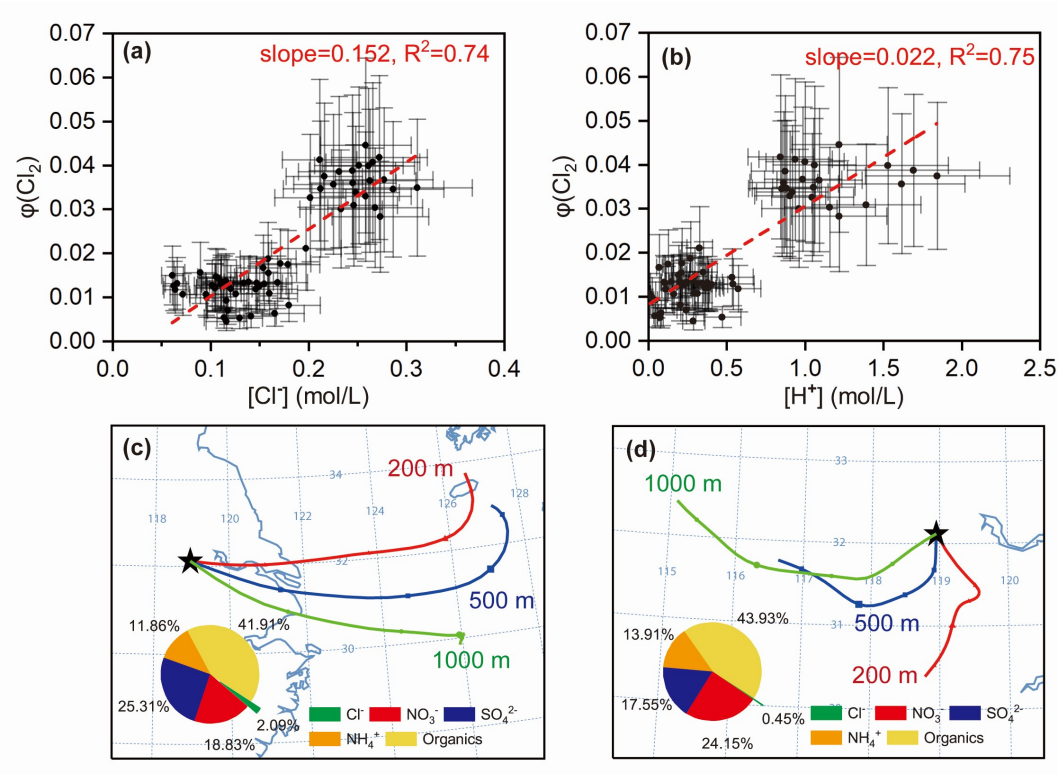

Figure 8. Estimated $\varphi(Cl_2)$ from N_2O_5 uptake and the factors influencing $\varphi(Cl_2)$ **(a)** and **(b)** Dependencies of $\varphi(Cl_2)$ on $[Cl^-]$ and $[H^+]$ in selected cases. **(c)** and **(d)** are examples of high

$\varphi(Cl_2)$ values in marine air masses (e.g., 13 April) and low $\varphi(Cl_2)$ values in inland air masses (e.g., 18 April) represented by 24-hour backward trajectories (see Fig. S2 for trajectories during the whole observations). Inserted pie charts show average aerosol chemical compositions during 21:40 on 12 April to 00:40 on 13 April and from 22:20 to 23:40 17 April, respectively.

A parameterization scheme is derived based on the dependences of $\varphi(Cl_2)$ on $[Cl^-]$ and $[H^+]$ to predict the Cl_2 formation involving N_2O_5 heterogeneous chemistry. Mechanistically, it is assumed that the nocturnal Cl_2 is produced from reactions involving NO_2^+ that can be produced either from uptake of N_2O_5 or $ClNO_2$. The production rates of nitrate, $ClNO_2$, and Cl_2 from the loss of NO_2^+ are expressed in Eq. (15) through Eq. (17). The loss rate of aerosol organics induced by NO_2^+ is expressed in Eq. (18) (noted as d[Org]/dt here).

$$d[NO_3^-]/dt = k_3[NO_2^+][H_2O] \quad (15)$$

$$d[ClNO_2]/dt = k_4[NO_2^+][Cl^-] \quad (16)$$

$$d[Cl_2]/dt = k_6[NO_2^+][Cl^-][H^+] \quad (17)$$

$$d[Org]/dt = k_5[NO_2^+][Org] \quad (18)$$

The symbol k_6 represents the rate constant of the reaction involving NO_2^+, Cl^-, and H^+. $\varphi(Cl_2)$ is obtained as follows, by assuming a steady state of the NO_2^+ intermediate (Bertram and Thornton, 2009) (Eq. (19)).

$$\varphi(Cl_2) = \frac{\frac{d[Cl_2]}{dt}}{\frac{d[Cl_2]}{dt} + \frac{d[ClNO_2]}{dt} + \frac{d[NO_3^-]}{dt} + \frac{d[Org]}{dt}} = \frac{k_6[Cl^-][H^+]}{k_6[Cl^-][H^+] + k_4[Cl^-] + k_3[H_2O] + k_5[Org]} \quad (19)$$

To remain consistent with the $\varphi(ClNO_2)$ parameterization, the values 483 and 2.05 were adopted for k_4/k_3 and k_5/k_3, respectively, while k_6/k_3 was estimated from the fitting of $\varphi(Cl_2)$ using Eq. (19) to achieve the least-squares errors between the observed and parameterized $\varphi(Cl_2)$ values. The parameterization of $\varphi(Cl_2)$ was then expressed as follows (Eq. (20)):

$$\varphi(Cl_2) = \frac{19.38[H^+][Cl^-]}{19.38[H^+][Cl^-] + 483[Cl^-] + [H_2O] + 2.05[Org]} \quad (20)$$

where the units of $[H^+]$, $[Cl^-]$, and [Org] are mol/L.

The previous $ClNO_2$ uptake method assumed a unity Cl_2 yield from $ClNO_2$ uptake, but no such assumption is required in the new method for an explicit definition (Eq. 14) and

parameterization (Eq. 20) of the $\varphi(Cl_2)$. In addition, a quantitative relationship between $\varphi(Cl_2)$ and aerosol acidity is established, which was not given in the previous parameterization. We recommend that air quality models test this parameterization for reproduction of nighttime Cl_2 observations.

4. Summary and conclusions

This study reports the presence of significant levels of $ClNO_2$ and Cl_2 at a suburban site in east China. A rapid increase in the $ClNO_2$ mixing ratios was found to occur after midnight due to larger rates of N_2O_5 heterogeneous loss than in early nighttime hours, and a high $\varphi(ClNO_2)$ value was also responsible for the elevated $ClNO_2$ mixing ratios. Improved parameterization of $\varphi(ClNO_2)$ at low to moderate range was achieved by involving the suppression effect of aerosol organics. We propose that the observed nighttime Cl_2 was a co-produced with $ClNO_2$ from the heterogeneous N_2O_5 uptake on acidic aerosols that bear chloride and suggest a mechanism for simultaneous production of $ClNO_2$ and Cl_2 from N_2O_5 hydrolysis. We have proposed a parameterization for $\varphi(Cl_2)$ from N_2O_5 uptake. The combination of $\varphi(Cl_2)$, $\varphi(ClNO_2)$, and $\gamma(N_2O_5)$ can be used in air quality models to predict the nighttime formation of Cl_2 and $ClNO_2$ from N_2O_5 uptake and their effect on the next day's atmospheric photochemistry.

Acknowledgments. This study was supported by the National Natural Science Foundation of China (NSFC) project (grant number: 91544213 and D0512/41675145), and the Hong Kong Research Grants Council (T24-504/17-N). The authors acknowledge helpful opinions and discussions from Dr. Yee Jun Tham.

Author contributions. TW designed the research. WN and AD managed the sampling sites. MX, XP, and WW performed the CIMS measurements. CY, ZX, PS, YL, YL, ZX provided other data. MX and TW wrote the manuscript with comments from all co-authors.

Competing interests. The authors declare that they have no conflict of interest.

Data availability. To request the CIMS, jNO_2, and NO_y data described in this study, please contact the corresponding author (cetwang@polyu.edu.hk). Other datasets are available by contacting Dr. Wei Nie (niewei@nju.edu.cn).

538

539 **References**

540 Ammann, M., Cox, R. A., Crowley, J. N., Jenkin, M. E., Mellouki, A., Rossi, M. J., Troe, J.,
541 and Wallington, T. J.: Evaluated kinetic and photochemical data for atmospheric chemistry:
542 Volume VI – heterogeneous reactions with liquid substrates, Atmos. Chem. Phys., 13, 8045-
543 8228, 10.5194/acp-13-8045-2013, 2013.
544 Baird, N. C., and Taylor, K. F.: The stabilizing effect of d orbitals on the central nitrogen atom
545 in nitrogen-oxygen molecules and ions, Chemical Physics Letters, 80, 83-86,
546 https://doi.org/10.1016/0009-2614(81)80062-0, 1981.
547 Behnke, W., George, C., Scheer, V., and Zetzsch, C.: Production and decay of $ClNO_2$ from the
548 reaction of gaseous N_2O_5 with NaCl solution: Bulk and aerosol experiments, Journal of
549 Geophysical Research: Atmospheres, 102, 3795-3804, 1997.
550 Bertram, T., and Thornton, J.: Toward a general parameterization of N_2O_5 reactivity on aqueous
551 particles: the competing effects of particle liquid water, nitrate and chloride, Atmospheric
552 Chemistry and Physics, 9, 8351-8363, 2009.
553 Breton, M. L., Hallquist, Å. M., Pathak, R. K., Simpson, D., Wang, Y., Johansson, J., Zheng, J.,
554 Yang, Y., Shang, D., and Wang, H.: Chlorine oxidation of VOCs at a semi-rural site in Beijing:
555 significant chlorine liberation from $ClNO_2$ and subsequent gas-and particle-phase Cl–VOC
556 production, Atmospheric Chemistry and Physics, 18, 13013-13030, 2018.
557 Custard, K. D., Pratt, K. A., Wang, S., and Shepson, P. B.: Constraints on Arctic Atmospheric
558 Chlorine Production through Measurements and Simulations of Cl_2 and ClO, Environmental
559 Science & Technology, 50, 12394-12400, 10.1021/acs.est.6b03909, 2016.
560 Deiber, G., George, C., Calvé, S. L., Schweitzer, F., and Mirabel, P.: Uptake study of $ClONO_2$
561 and $BrONO_2$ by Halide containing droplets, Atmospheric Chemistry and Physics, 4, 1291-1299,
562 2004.
563 Ding, A., Fu, C., Yang, X., Sun, J., Zheng, L., Xie, Y., Herrmann, E., Nie, W., Petäjä, T., and
564 Kerminen, V.-M.: Ozone and fine particle in the western Yangtze River Delta: an overview of
565 1 yr data at the SORPES station, Atmospheric Chemistry and Physics, 13, 5813-5830, 2013.
566 Ding, A., Huang, X., Nie, W., Chi, X., Xu, Z., Zheng, L., Xu, Z., Xie, Y., Qi, X., and Shen, Y.:
567 Significant reduction of $PM_{2.5}$ in eastern China due to regional-scale emission control: evidence
568 from SORPES in 2011–2018, Atmospheric Chemistry and Physics, 19, 11791-11801, 2019.
569 Finlayson-Pitts, B., Ezell, M., and Pitts, J.: Formation of chemically active chlorine compounds
570 by reactions of atmospheric NaCl particles with gaseous N_2O_5 and $ClONO_2$, Nature, 337, 241-
571 244, 1989.
572 Haskins, J. D., Lee, B. H., Lopez-Hilifiker, F. D., Peng, Q., Jaeglé, L., Reeves, J. M., Schroder,
573 J. C., Campuzano-Jost, P., Fibiger, D., and McDuffie, E. E.: Observational constraints on the
574 formation of Cl_2 from the reactive uptake of $ClNO_2$ on aerosols in the polluted marine boundary
575 layer, Journal of Geophysical Research: Atmospheres, 124, 8851-8869, 2019.
576 Kercher, J., Riedel, T., and Thornton, J.: Chlorine activation by N_2O_5: simultaneous, in situ
577 detection of $ClNO_2$ and N_2O_5 by chemical ionization mass spectrometry, Atmospheric
578 Measurement Techniques, 2, 193-204, 2009.

Lewis, E. R.: An examination of Köhler theory resulting in an accurate expression for the equilibrium radius ratio of a hygroscopic aerosol particle valid up to and including relative humidity 100%, Journal of Geophysical Research: Atmospheres, 113, 2008.
Liao, J., Huey, L. G., Liu, Z., Tanner, D. J., Cantrell, C. A., Orlando, J. J., Flocke, F. M., Shepson, P. B., Weinheimer, A. J., and Hall, S. R.: High levels of molecular chlorine in the Arctic atmosphere, Nature Geoscience, 7, 91, 2014.
Liu, X., Qu, H., Huey, L. G., Wang, Y., Sjostedt, S., Zeng, L., Lu, K., Wu, Y., Hu, M., and Shao, M.: High levels of daytime molecular chlorine and nitryl chloride at a rural site on the North China Plain, Environmental science & technology, 51, 9588-9595, 2017.
Li, Y., Nie, W., Liu, Y., Huang, D., Xu, Z., Peng, X., George, C., Yan, C., Tham, Y. J., Yu, C., Xia, M., Fu, X., Wang, X., Xue, L., Wang, Z., Xu, Z., Chi, X., Wang, T., and Ding, A.: Photoinduced Production of Chlorine Molecules from Titanium Dioxide Surfaces Containing Chloride, Environmental Science & Technology Letters, 7, 70-75, 10.1021/acs.estlett.9b00704, 2020.
McDuffie, E. E., Fibiger, D. L., Dubé, W. P., Lopez-Hilfiker, F., Lee, B. H., Thornton, J. A., Shah, V., Jaeglé, L., Guo, H., and Weber, R. J.: Heterogeneous N_2O_5 uptake during winter: Aircraft measurements during the 2015 WINTER campaign and critical evaluation of current parameterizations, Journal of Geophysical Research: Atmospheres, 123, 4345-4372, 2018a.
McDuffie, E. E., Fibiger, D. L., Dubé, W. P., Lopez Hilfiker, F., Lee, B. H., Jaeglé, L., Guo, H., Weber, R. J., Reeves, J. M., and Weinheimer, A. J.: $ClNO_2$ yields from aircraft measurements during the 2015 WINTER campaign and critical evaluation of the current parameterization, Journal of Geophysical Research: Atmospheres, 123, 12,994-913,015, 2018b.
McNamara, S. M., Raso, A. R., Wang, S., Thanekar, S., Boone, E. J., Kolesar, K. R., Peterson, P. K., Simpson, W. R., Fuentes, J. D., and Shepson, P. B.: Springtime Nitrogen Oxide-Influenced Chlorine Chemistry in the Coastal Arctic, Environmental science & technology, 2019.
Mielke, L. H., Furgeson, A., and Osthoff, H. D.: Observation of $ClNO_2$ in a mid-continental urban environment, Environ Sci Technol, 45, 8889-8896, 10.1021/es201955u, 2011.
Molina, M. J., and Rowland, F. S.: Stratospheric sink for chlorofluoromethanes: chlorine atom-catalysed destruction of ozone, Nature, 249, 810, 1974.
Morgan, W., Ouyang, B., Allan, J., Aruffo, E., Di Carlo, P., Kennedy, O., Lowe, D., Flynn, M., Rosenberg, P., and Williams, P.: Influence of aerosol chemical composition on N_2O_5 uptake: airborne regional measurements in northwestern Europe, Atmospheric Chemistry and Physics, 15, 973-990, 2015.
Osthoff, H. D., Roberts, J. M., Ravishankara, A. R., Williams, E. J., Lerner, B. M., Sommariva, R., Bates, T. S., Coffman, D., Quinn, P. K., Dibb, J. E., Stark, H., Burkholder, J. B., Talukdar, R. K., Meagher, J., Fehsenfeld, F. C., and Brown, S. S.: High levels of nitryl chloride in the polluted subtropical marine boundary layer, Nature Geoscience, 1, 324-328, 10.1038/ngeo177, 2008.
Phillips, G. J., Thieser, J., Tang, M., Sobanski, N., Schuster, G., Fachinger, J., Drewnick, F., Borrmann, S., Bingemer, H., and Lelieveld, J.: Estimating N_2O_5 uptake coefficients using ambient measurements of NO_3, N_2O_5, $ClNO_2$ and particle-phase nitrate, Atmospheric

Chemistry and Physics, 16, 13231-13249, 2016.
Pratte, P., and Rossi, M. J.: The heterogeneous kinetics of HOBr and HOCl on acidified sea salt and model aerosol at 40–90% relative humidity and ambient temperature, Physical Chemistry Chemical Physics, 8, 3988-4001, 2006.
Priestley, M., Breton, M. l., Bannan, T. J., Worrall, S. D., Bacak, A., Smedley, A. R., Reyes-Villegas, E., Mehra, A., Allan, J., and Webb, A. R.: Observations of organic and inorganic chlorinated compounds and their contribution to chlorine radical concentrations in an urban environment in northern Europe during the wintertime, Atmospheric Chemistry and Physics, 18, 13481-13493, 2018.
Qiu, X., Ying, Q., Wang, S., Duan, L., Zhao, J., Xing, J., Ding, D., Sun, Y., Liu, B., and Shi, A.: Modeling the impact of heterogeneous reactions of chlorine on summertime nitrate formation in Beijing, China, Atmospheric Chemistry and Physics, 19, 6737-6747, 2019.
Riedel, T. P., Bertram, T. H., Crisp, T. A., Williams, E. J., Lerner, B. M., Vlasenko, A., Li, S. M., Gilman, J., de Gouw, J., Bon, D. M., Wagner, N. L., Brown, S. S., and Thornton, J. A.: Nitryl chloride and molecular chlorine in the coastal marine boundary layer, Environ Sci Technol, 46, 10463-10470, 10.1021/es204632r, 2012.
Riedel, T. P., Wagner, N. L., Dubé, W. P., Middlebrook, A. M., Young, C. J., Öztürk, F., Bahreini, R., VandenBoer, T. C., Wolfe, D. E., and Williams, E. J.: Chlorine activation within urban or power plant plumes: Vertically resolved $ClNO_2$ and Cl_2 measurements from a tall tower in a polluted continental setting, Journal of Geophysical Research: Atmospheres, 118, 8702-8715, 2013.
Roberts, J. M., Osthoff, H. D., Brown, S. S., and Ravishankara, A.: N_2O_5 oxidizes chloride to Cl_2 in acidic atmospheric aerosol, Science, 321, 1059-1059, 2008.
Roberts, J. M., Osthoff, H. D., Brown, S. S., Ravishankara, A., Coffman, D., Quinn, P., and Bates, T.: Laboratory studies of products of N_2O_5 uptake on Cl^- containing substrates, Geophysical Research Letters, 36, 2009.
Seinfeld, J. H., and Pandis, S. N.: Atmospheric chemistry and physics: from air pollution to climate change, John Wiley & Sons, 2016.
Simpson, W. R., Brown, S. S., Saiz-Lopez, A., Thornton, J. A., and von Glasow, R.: Tropospheric halogen chemistry: Sources, cycling, and impacts, Chemical reviews, 115, 4035-4062, 2015.
Spicer, C., Chapman, E., Finlayson-Pitts, B., Plastridge, R., Hubbe, J., Fast, J., and Berkowitz, C.: Unexpectedly high concentrations of molecular chlorine in coastal air, Nature, 394, 353, 1998.
Staudt, S., Gord, J. R., Karimova, N., McDuffie, E. E., Brown, S. S., Gerber, R. B., Nathanson, G. M., and Bertram, T. H.: Sulfate and Carboxylate Suppress the Formation of $ClNO_2$ at Atmospheric Interfaces, ACS Earth and Space Chemistry, 2019.
Sun, P., Nie, W., Chi, X., Xie, Y., Huang, X., Xu, Z., Qi, X., Xu, Z., Wang, L., and Wang, T.: Two years of online measurement of fine particulate nitrate in the western Yangtze River Delta: influences of thermodynamics and N_2O_5 hydrolysis, Atmospheric Chemistry and Physics, 18, 17177-17190, 2018.
Taylor, R., Electrophilic Aromatic Substitution, John Wiley, New York, 1990.

Tham, Y. J., Wang, Z., Li, Q., Yun, H., Wang, W., Wang, X., Xue, L., Lu, K., Ma, N., Bohn, B., Li, X., Kecorius, S., Größ, J., Shao, M., Wiedensohler, A., Zhang, Y., and Wang, T.: Significant concentrations of nitryl chloride sustained in the morning: investigations of the causes and impacts on ozone production in a polluted region of northern China, Atmospheric Chemistry and Physics, 16, 14959-14977, 10.5194/acp-16-14959-2016, 2016.

Tham, Y. J., Wang, Z., Li, Q., Wang, W., Wang, X., Lu, K., Ma, N., Yan, C., Kecorius, S., and Wiedensohler, A.: Heterogeneous N_2O_5 uptake coefficient and production yield of $ClNO_2$ in polluted northern China: Roles of aerosol water content and chemical composition, 2018.

Thornton, J. A., Braban, C. F., and Abbatt, J. P.: N_2O_5 hydrolysis on sub-micron organic aerosols: The effect of relative humidity, particle phase, and particle size, Physical Chemistry Chemical Physics, 5, 4593-4603, 2003.

Thornton, J. A., Kercher, J. P., Riedel, T. P., Wagner, N. L., Cozic, J., Holloway, J. S., Dube, W. P., Wolfe, G. M., Quinn, P. K., Middlebrook, A. M., Alexander, B., and Brown, S. S.: A large atomic chlorine source inferred from mid-continental reactive nitrogen chemistry, Nature, 464, 271-274, 10.1038/nature08905, 2010.

Wang, T., Tham, Y. J., Xue, L., Li, Q., Zha, Q., Wang, Z., Poon, S. C., Dubé, W. P., Blake, D. R., and Louie, P. K.: Observations of nitryl chloride and modeling its source and effect on ozone in the planetary boundary layer of southern China, Journal of Geophysical Research: Atmospheres, 121, 2476-2489, 2016.

Wang, X., Jacob, D. J., Eastham, S. D., Sulprizio, M. P., Zhu, L., Chen, Q., Alexander, B., Sherwen, T., Evans, M. J., Lee, B. H., Haskins, J. D., Lopez-Hilfiker, F. D., Thornton, J. A., Huey, G. L., and Liao, H.: The role of chlorine in global tropospheric chemistry, Atmos. Chem. Phys., 19, 3981-4003, 10.5194/acp-19-3981-2019, 2019.

Wexler, A. S.: Atmospheric aerosol models for systems including the ions H^+, NH_4^+, Na^+, SO_4^{2-}, NO_3^-, Cl^-, Br^-, and H_2O, Journal of Geophysical Research, 107, 10.1029/2001jd000451, 2002.

Yun, H., Wang, W., Wang, T., Xia, M., Yu, C., Wang, Z., Poon, S. C., Yue, D., and Zhou, Y.: Nitrate formation from heterogeneous uptake of dinitrogen pentoxide during a severe winter haze in southern China, Atmospheric Chemistry and Physics, 18, 17515-17527, 2018.

Zhou, Y., Zhao, Y., Mao, P., Zhang, Q., Zhang, J., Qiu, L., and Yang, Y.: Development of a high-resolution emission inventory and its evaluation and application through air quality modeling for Jiangsu Province, China, Atmospheric Chemistry and Physics, 17, 211-233, 2017.